Near-Infrared Spectroscopic Cathodoluminescence Imaging Polarimetry on Silicon Photonic Crystal Waveguides

Benjamin J. M. Brenny,[†] Daryl M. Beggs,[‡,§] Ruben E. C. van der Wel,[†] L. Kuipers,[†] and Albert Polman*[,†]

[†]Center for Nanophotonics, FOM Institute AMOLF, Science Park 104, 1098 XG Amsterdam, The Netherlands
[‡]Centre for Quantum Photonics, H.H. Wills Physics Laboratory, University of Bristol, Tyndall Avenue, Bristol BS8 1TL, United Kingdom
[§]School of Physics and Astronomy, Cardiff University, Cardiff CF24 3AA, United Kingdom

ⓢ *Supporting Information*

ABSTRACT: We measure polarization- and wavelength-resolved spectra and spatial emission intensity distributions from silicon photonic crystal waveguides in the near-infrared spectral range using spectroscopic cathodoluminescence imaging polarimetry. A 30 keV electron beam, incident along the surface normal of the sample, acts as an ultrabroadband and deeply subwavelength excitation source. For photonic crystal waveguides with a broad range of design parameters, we observe a dominant emission intensity distribution that is strongly confined to the waveguide. For a period of 420 nm and a hole radius of 120 nm, this occurs at a wavelength of 1425 nm. The polarization-resolved measurements demonstrate that this feature is fully linearly polarized along the waveguide axis. Comparing the modal pattern and polarization to calculations of the electric field profiles confirms that we measure the odd TE waveguide mode of the system. This result demonstrates that the electron beam can couple to modes dominated by in-plane field components in addition to the more commonly observed modes dominated by out-of-plane field components. From the emission directionality, we conclude that we sample a leaky portion of the odd waveguide mode.

KEYWORDS: *cathodoluminescence, photonic crystal waveguide, polarimetry, near-infrared*
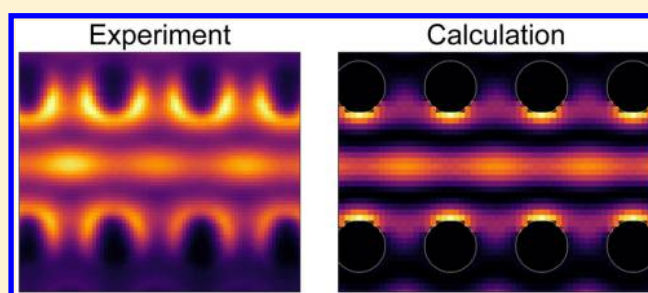
Photonic crystals, materials with a periodically varying dielectric function, can manipulate the propagation of light in a controlled way. They create a photonic band gap that prevents light from propagating in certain directions for certain frequencies.[1−5] The photonic band gap can lead to a strong confinement of light, and engineered defects allow the creation of photonic crystal cavities and waveguides. Photonic crystal cavities can have long photon lifetimes and small mode volumes,[6−8] leading to strong light−matter interactions and enabling applications such as low threshold lasers.[9−12] Photonic crystal waveguides are strongly dispersive and can slow light down, which also leads to enhanced light−matter interactions.[13−21] This strong dispersion allows such waveguides to serve as many components and building blocks in photonic integrated circuits, such as splitters, switches, or multiplexers.[18,22−25] To fully exploit the many applications of photonic crystal waveguides, it is essential to measure the propagation and confinement of light at a subwavelength scale. This cannot be achieved by conventional microscopy techniques. Near-field scanning optical microscopy (NSOM), which uses subwavelength probes or apertures to detect or scatter the near field of these structures,[26−30] has enabled measurements of the field components of the optical near field just above the waveguide.[31,32]

Cathodoluminescence (CL) spectroscopy is an alternative technique that can be used to study nanophotonic structures, coupling to and probing the field distributions inside. A high-energy electron beam is used as a nanoscale optical excitation source in which the time-varying electromagnetic field of the electron couples to the local optical modes of the system as it traverses the sample.[33−35] This mechanism, which is fully described by Maxwell's equations, is fundamentally similar to that of the oscillating electric field of a laser beam coupling to optical excitations. In CL, the light scattered from these optical modes to the far field is detected. The short interaction time of the electron with the structure (a few femtoseconds) results in a broadband excitation spectrum (typically several micrometers, down into the deep UV). The high excitation resolution of CL is limited only by the extent of the electric field about the electron trajectory and the spread of the beam in the sample. This allows one to explore the radiative local density of optical states (LDOS) at deeply subwavelength scales.[34,36] The electron forms a noninvasive probe of the optical properties inside the material. Recently, it has become possible to measure the full polarization distribution of CL emission as a function of
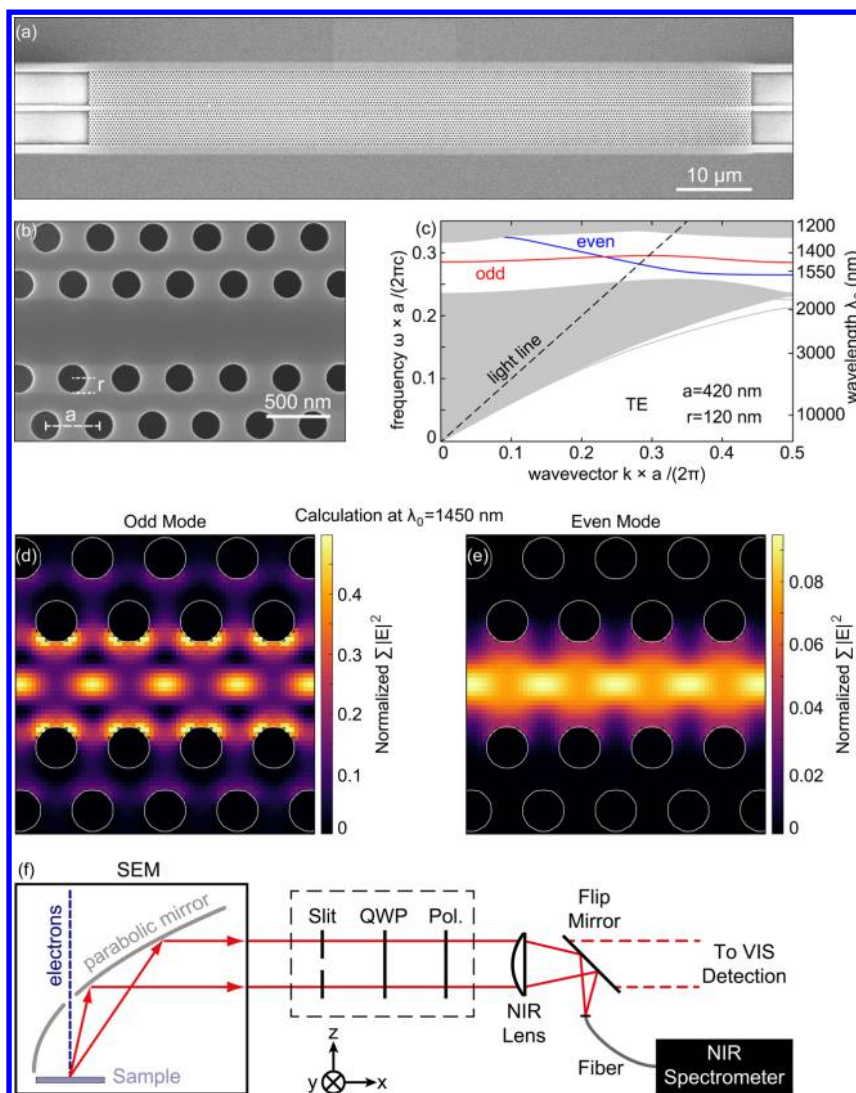
Figure 1. (a) Scanning electron micrograph of one of the silicon PCWGs on sample 1 studied here. A 90 μm long, 10 μm wide, and 220 nm thick waveguide with a hexagonal lattice of holes is suspended above a substrate of silica on silicon. (b) Close-up micrograph of waveguide WG2, with a period of a = 420 nm and a hole radius of r = 120 nm. (c) Band diagram of the waveguide from (b) for TE polarization. The gray regions denote the continuum of available modes above and below the photonic band gap, within which we distinguish an even (blue) and odd (red) waveguide mode. The black dashed line corresponds to the light line of air. (d, e) Calculation of the modal intensity distributions of the odd (e) and even (f) waveguide modes, for λ_0 = 1450 nm, normalized to the maximum intensity for all polarizations and wavelengths. The white circles show the positions of the holes. (f) Schematic of the cathodoluminescence spectroscopy system. The 30 keV electron beam excites the sample; a parabolic mirror collects the emitted radiation and directs it to an optical setup. Here we can focus the light onto a NIR spectrometer or filter the emitted beam with a (vertically oriented) slit and measure the full polarization state using a quarter-wave plate and linear polarizer. The PCWGs for all measurements in the main text are oriented along the y-axis of the coordinate system.

angle by using polarimetry.[37] These properties have made CL a powerful, deeply subwavelength characterization technique,[38−44] allowing measurements of the confinement and dispersion of plasmonic and dielectric photonic crystal cavities in the visible spectral range.[34,45−47]

In this article, we apply spectroscopic cathodoluminescence imaging polarimetry in the near-infrared (NIR) spectral range to study the confinement and polarization of propagating photonic crystal waveguide modes. More specifically, we examine how the electron beam couples to the electromagnetic eigenmodes of the system. CL emission is typically dominated by modes with primarily out-of-plane electric field components (hereafter referred to as out-of-plane or TM modes). Modes with primarily in-plane electric field components (hereafter referred to as in-plane or TE modes) are usually not significant.

These structures, however, possess different band structures for TE and TM polarization and support two well-defined modes for TE polarization, denoted as even and odd.[5,48,49] We demonstrate that CL imaging polarimetry enables direct identification and spatial mapping of the modal field distribution in the photonic crystal waveguides. The CL emission is dominated by the odd TE waveguide mode, with measurements showing good agreement with calculations of the modal field intensities. Using photonic crystal waveguides as a well-known model system, we demonstrate the direct excitation of in-plane TE modes by the electron beam. We show that the excitation process involves a complex combination of coupling of the electron beam to multiple field components of the propagating TE modes.

■ EXPERIMENT

Silicon photonic crystal waveguides (PCWGs) were fabricated on silicon-on-insulator wafers with a 220 nm thick silicon layer on top of a 1 μm silica layer on a silicon substrate. Electron beam lithography was used to pattern the waveguides, followed by reactive ion etching to etch through the top silicon layer. A wet HF etch was used to remove part of the silica layer and obtain a suspended PCWG. Reference measurements in the visible and NIR spectral ranges demonstrate that a residual silica layer remains, since we observe characteristic silica defect-related emission peaks. Two different samples were studied; here we discuss only sample 1, showing data for sample 2 in Figure S1 of the Supporting Information. Figure 1a shows a SEM image of one of the PCWGs on sample 1 examined here, with a length of 90 μm and a total width of the photonic crystal section of 10 μm. The PCWG is composed of a hexagonal array of holes with one missing row of holes (W1 waveguide).[5,49,50] Five waveguides were made on sample 1 with the same period a = 420 nm and hole radii varying in the range ∼105−125 nm. Figure 1b shows a close-up of the waveguide section for the most studied structure (denoted as WG2), which has a period a = 420 nm and a hole radius r = 120 nm.

The TE band structure of WG2 is shown in Figure 1c, calculated using an open-source MIT Photonic Bands (MPB) frequency domain mode-solver.[51] TE polarization corresponds to electric fields that are primarily oriented in the plane of the waveguide slab (fully so only in the vertical plane of symmetry z = 0). The gray bands represent modes that make up a continuum below and above the photonic band gap, which opens up between normalized frequencies of ∼0.25−0.32, corresponding to free space wavelengths of ca. λ_0 = 1300−1700 nm. The discrete bands at the lower right are index-guided bands,[5] confined by total internal reflection in the slab. The band structure is very sensitive to the period, hole size, and slab thickness.[52]

Removing rows of holes leads to allowed modes within this band gap,[48−50,53] that are confined vertically by index-guiding (total internal reflection), but horizontally by the band gap of the photonic crystal. For a single row of missing holes there are two TE waveguide modes in the band gap: an even mode with a symmetric field distribution and an odd mode with an antisymmetric distribution for the in-plane transverse electric field component.[13,48] The even mode has been studied intensely due to its anomalous dispersion and vanishing group velocity over a large range of wavevectors when approaching the edge of the Brillouin zone.[13,14,18,19] The odd mode is less well studied, but also displays slow light over a broad range of wavevectors (see Figure 1c). The dashed line in the figure represents the light line in air; modes to the left will be leaky and modes to the right are guided in the waveguide slab.

In addition to TE modes, the photonic crystal possesses TM modes, with an electric field perpendicular to the waveguide slab at z = 0. Such modes are usually excited efficiently by CL,[33] since the moving electron acts as a vertically polarized source. In Figure S4 of the Supporting Information we show the band structure for TM polarization. We find that there is a small photonic band gap for wavelengths in the range of ca. λ_0 = 1100−1200 nm with two waveguide modes within. In the spectral range of the TE band gap, the TM band structure exhibits a continuum of modes. Modes inside or near the band gap are usually localized to the waveguide, while modes in the

continuous bands are more delocalized over the photonic crystal.[5,48] The PCWGs studied here are specifically designed for high-quality TE modes rather than TM modes, so the former will typically exhibit a higher LDOS. There are thus multiple possible sources of emission, for both TE and TM polarization, when exciting these Si PCWGs with swift electrons.

Figure 1d,e show calculations of the electric field intensity distributions for the odd (d) and even (e) TE-polarized modes at λ_0 = 1450 nm, using the MPB code. We calculate the E_x, E_y, and E_z field components as a function of position and wavevector within a small frequency range, then integrate over all k and field components. For simplicity, these calculations are all 2D, performed at z = 0 so E_z is strictly 0 as well, but this does not affect the relevant features of these in-plane modes (see Figure S5 of the Supporting Information for 3D calculations of E_z). All 2D calculations are normalized to the same overall maximum (obtained for TE at λ_0 = 1500 nm, not shown here) and the holes are masked (the intensity inside the holes is set to zero) to better compare the results to the measurements. For more details about the calculation procedure, see the Methods section. We observe that both odd (Figure 1d) and even (Figure 1e) modes display sharp high-intensity features along the center of the waveguide. The odd mode, however, exhibits a more localized, distinct, and bright modal distribution pattern. These two modes are differentiated by the symmetry of the in-plane field component transverse to the waveguide propagation direction, which becomes clear when examining the real or imaginary amplitudes (not shown here) but not apparent for the field intensity presented here. The modes are, however, also dominated by different field components (see Figure S7 of the Supporting Information).

Calculations for TM polarization in the range λ_0 = 1430−1500 nm are shown in Figure S4 of the Supporting Information, but exhibit no sharp features such as the ones on display for TE polarization.

Figure 1f depicts a schematic representation of the CL setup.[34,37,54] The 30 keV electron beam excites the sample, and a parabolic mirror collects the subsequent emission and directs it onto a fiber connected to a NIR spectrometer. The small size of the electron probe and precise scanning capabilities of the SEM allow us to perform spectrally and spatially resolved scans of the PCWGs. We also measure the spectrally resolved polarization of the emission by adding a movable, vertical slit to the optical path. In general, the polarization of the emitted radiation can change as it reflects off the mirror, due to its curved shape. The slit selects the central part of the mirror and conserves the emission polarization,[55,56] integrating over zenithal angles for a narrow range of azimuthal angles. We perform measurements for different positions of the slit and orientations of the waveguide with respect to the mirror to determine the polarization state and emission directionality (see Supporting Information). We combine a quarter-wave plate (QWP) and linear polarizer (Pol.) to determine the Stokes parameters, which fully describe the polarization state of the emitted light.[37,57] This allows for the separation of polarized and unpolarized light, as well as the retrieval of different field components inside the structure and the relative phase difference between them.[57] Measuring the emission polarization thus allows the mapping of the electric field components. The Methods section describes the experimental setup and measurement protocol in more detail. For the
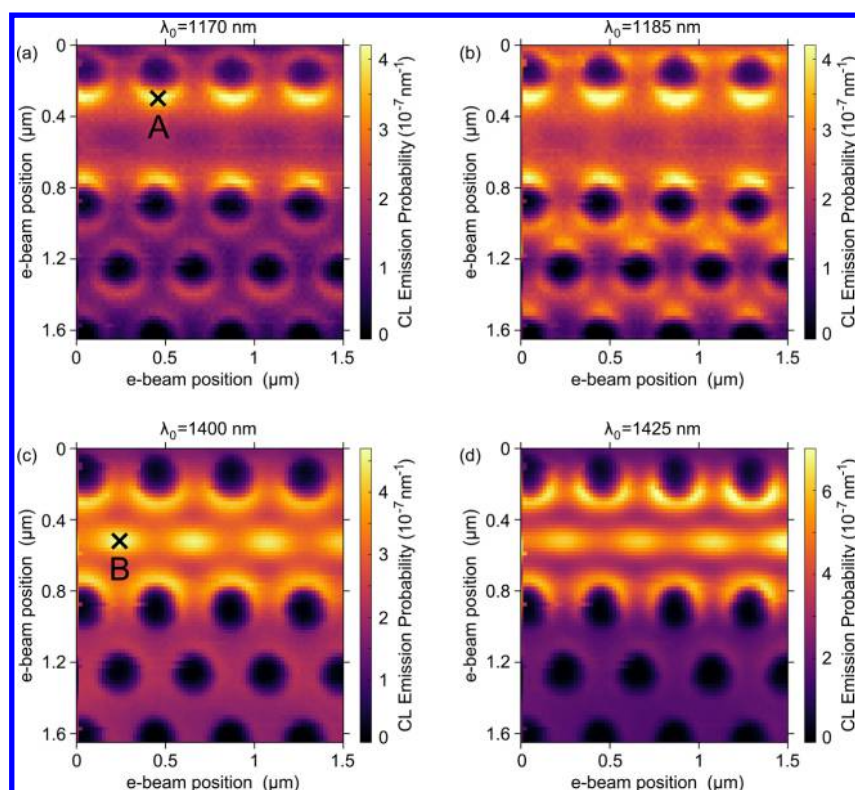
Figure 2. Measured CL emission probability of WG2, as a function of wavelength and excitation position, for center wavelengths of $\lambda_0 = 1170$ nm (a), $\lambda_0 = 1185$ nm (b), $\lambda_0 = 1400$ nm (c), and $\lambda_0 = 1425$ nm (d) (20 nm bandwidth). Black crosses denote the two locations for which we show spectra in Figure 3.

measurements described in the main text, all waveguides are oriented along the *y*-axis, as defined by the coordinate system in Figure 1f.

■ NEAR-INFRARED SPATIALLY RESOLVED CATHODOLUMINESCENCE

Figure 2 presents 2D spatial CL intensity maps from WG2, at wavelengths of $\lambda_0 = 1170$ nm (a), $\lambda_0 = 1185$ nm (b), $\lambda_0 = 1400$ nm (c), and $\lambda_0 = 1425$ nm (d), all averaged over a 20 nm bandwidth. Combining the raw data with the spectral response of the system and in situ beam current measurements allow us to determine the CL emission probability (number of photons emitted per incoming electron, per unit bandwidth of nm^{-1}).[58] We additionally correct the data for the dark response of the detector as well as for signal from the remaining silica and the silicon substrate, which contributes a broadband response and a peak at $\lambda_0 = 1275$ nm. To do so, we use a reference spectrum measured in one of the holes, which has no contribution from the waveguide or photonic crystal modes. In the Supporting Information, we show additional measurements for a sample with a different period (Figure S1), for the input section of WG2 (Figure S2) and for WG2 closer to the visible spectral range (Figure S3).

The measurements at $\lambda_0 = 1170$ nm and $\lambda_0 = 1185$ nm (Figure 2a,b) exhibit an overall similarity, with high intensity at the inner edges of the holes lining the waveguide and darker spots along the waveguide at positions in between four holes. These two positions are denoted as A and B in Figure 2a,c. Figure 2b exhibits a distinct enhanced intensity at the edges of the holes outside of the waveguide, compared to Figure 2a. Figure 2c,d show data at $\lambda_0 = 1400$ nm and $\lambda_0 = 1425$ nm, displaying a high intensity at the inner edges of the holes lining

the waveguide, which wrap around the hole edges more than for the data at shorter wavelengths. The center of the waveguide exhibits high-intensity features at positions that were dark for $\lambda_0 = 1170$ nm and $\lambda_0 = 1185$ nm. At $\lambda_0 = 1425$ nm these peaks are most intense, while the region around the waveguide has a lower relative intensity than for $\lambda_0 = 1400$ nm. The fact that the signal for $\lambda_0 = 1425$ nm is very strongly confined to the waveguide suggests it is related to a waveguide mode.

The features at $\lambda_0 = 1170$ nm and $\lambda_0 = 1185$ nm occur in the upper band of the TE band structure (see Figure 1c), which represent modes that are delocalized over the waveguide and surrounding holes,[5,48] as seen in Figure 2a,b. In addition to TE modes, TM modes could also be responsible for this measured emission. As Figure S4 of the Supporting Information demonstrates, there is a small TM photonic band gap for wavelengths in the range of ca. $\lambda_0 = 1100-1200$ nm with two waveguide modes within. The emission patterns at $\lambda_0 = 1400$ nm and $\lambda_0 = 1425$ nm occur in the middle of the TE photonic band gap, where the even and odd waveguide modes are present. For TM polarization these wavelengths are in the continuum of modes below the TM band gap, where one expects modes that are more delocalized from the waveguide, unlike the patterns observed here that are strongly confined to the waveguide. Comparing the measurements to the calculations of the modal field distributions in Figure 1d,e, excellent agreement is observed between the data and the odd TE waveguide mode, while calculations for TM polarization exhibit a very different and weaker response (Figure S4 of the Supporting Information). This indicates that the out-of-plane electron beam is coupling most strongly to an in-plane mode, which seems counterintuitive at first.

The electron beam principally couples to field components that are parallel to the electron trajectory.[33] For electrons propagating along z, this should lead to preferential coupling to the TM modes, yet we clearly observe patterns identical to TE modes. Our 2D calculations for TE polarization are performed at $z = 0$, where E_z is strictly zero. The membrane does have a finite thickness, however, so E_z has nonzero components for other z-coordinates.[5] We can, for example, expect vertical components at the edges of the holes.[32] To verify this, we have performed a set of 3D MPB calculations, determining the modal fields for different values of z. We display the calculated E_z in Figure S5 of the Supporting Information, showing that the hole edges indeed exhibit a distinct E_z component. Considering the high intensity in the middle of the waveguide, the even mode is symmetric with respect to the center, for the transverse in-plane field component (perpendicular to the waveguide axis), so there is no field gradient across the central axis and the electric field is expected to remain in-plane. The odd mode however is antisymmetric for the transverse in-plane field component, exhibiting a field gradient across the central axis and a node at the very center where the field switches sign. This flip in the fields is accompanied by a nonzero E_z component in the center for different (nonzero) z-coordinates, explaining why we preferentially measure the odd mode. This is also confirmed by Figure S5, showing that the odd mode has nonzero values of E_z along the waveguide center, while E_z of the even mode is close to zero and the odd mode also has a higher intensity overall than the even mode. The E_z intensity locally reaches ~15% of the maximum value of the total intensity for the odd mode and ~5% for the even mode.

Another source of coupling between the electrons and the TE modes is the fact that scattering of the incident electrons inside the silicon membrane leads to a spread in their propagation directions, allowing for direct coupling to in-plane field components.[34] The scattering increases for lower electron energies, which should result in stronger coupling to the in-plane components. We do indeed observe higher intensities from the modal peaks using 10 keV instead of 30 keV (not shown here).

Both the 3D distribution of the electric fields with locally significant E_z components aligned with the incident electrons and electron scattering inside the silicon slab allowing for alignment with the E_x and E_y components play a role in exciting the in-plane TE modes in the PCWG slab. Although TM modes should still have a better overlap with the electron beam, the band structure is dominated by a continuum of modes. For TE, however, there is a clear band gap with well-defined waveguide modes that can stand out, as they have a higher local density of states than the delocalized TM modes.

■ SPECTROSCOPIC POLARIMETRY

To further confirm the TE nature of the measured modes, we need to study the polarization-filtered spectral response of the waveguide. We begin by examining nonfiltered spectra in Figure 3a, which presents the CL spectra at the inner edge of the hole lining the waveguide (position A in Figure 2a, in red) and in the center of the waveguide between four holes (position B in Figure 2c, in blue). Both positions are dominated by a peak at $\lambda_0 \approx 1425$ nm. The spectrum for position A also exhibits additional smaller peaks at $\lambda_0 \approx 1225$ and 1175 nm, for which the CL intensity distribution was plotted in Figure 2a,b.

The modal structure of PCWGs is sensitive to small changes in the geometry, which is demonstrated in Figure 3b, where we
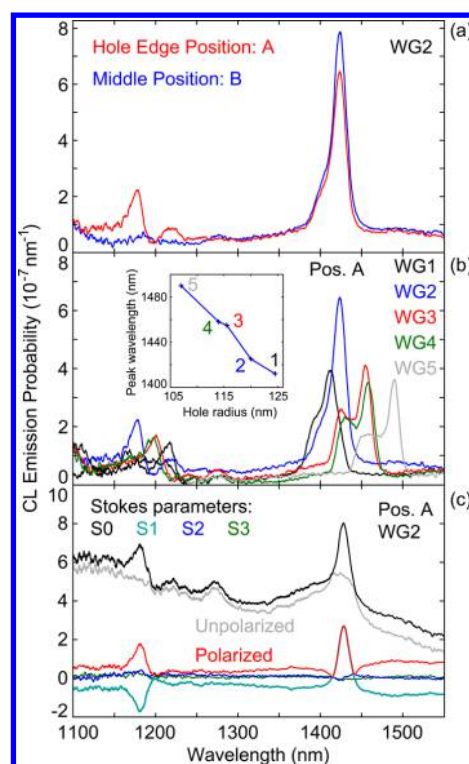

Figure 3. (a) CL emission probability as a function of wavelength, measured on WG2, comparing the spectra obtained for two different excitation positions, A (red) and B (blue), indicated in Figure 2. (b) CL spectra obtained for excitation position A on five different waveguides (WG1−WG5) with different hole size. The inset shows the wavelength of the dominant peak as a function of hole radius. (c) Polarization-filtered spectra measured on WG2 for excitation position A. We determine the Stokes parameters S0 (black), S1 (turquoise), S2 (blue), and S3 (green) and use them to separate the polarized contribution (red) from the unpolarized contribution that is due to the background luminescence from the substrate (gray). We note that S1 and the polarized contribution overlap at $\lambda_0 \approx 1425$ nm.

have measured the spectra for five different waveguides (WG1−WG5) with increasing hole sizes, all measured for excitation position A. We observe a clear red-shift of the spectral features for decreasing hole size. We note a variability in the intensity as well as an increasing contribution of a second peak on the blue side of the main emission peak for decreasing hole size. The inset of Figure 3b shows the main peak resonance wavelength as a function of the hole radius, as determined from SEM images. A ~20 nm change in hole radius leads to a ~80 nm shift in the resonance wavelength, underlining the sensitivity of the modes to geometrical parameters.[52]

To measure the polarization-resolved spectra, we first place the vertical movable slit with a width of 3 mm in the optical path. We find that both peaks at $\lambda_0 \approx 1175$ nm and $\lambda_0 \approx 1425$ nm in the spectra from Figure 3a exhibit maximum intensity in the middle of the mirror, for orthogonal orientations of the waveguide relative to the mirror, indicating that the emission direction is close to the surface normal. We can now use polarimetry to determine the polarization state of the emitted radiation, which allows the retrieval of the electric field orientations inside the structure. We assume the interface does not significantly alter the field orientations for emission close to the surface normal. For these measurements we do not separately subtract the signal from the substrate. More details
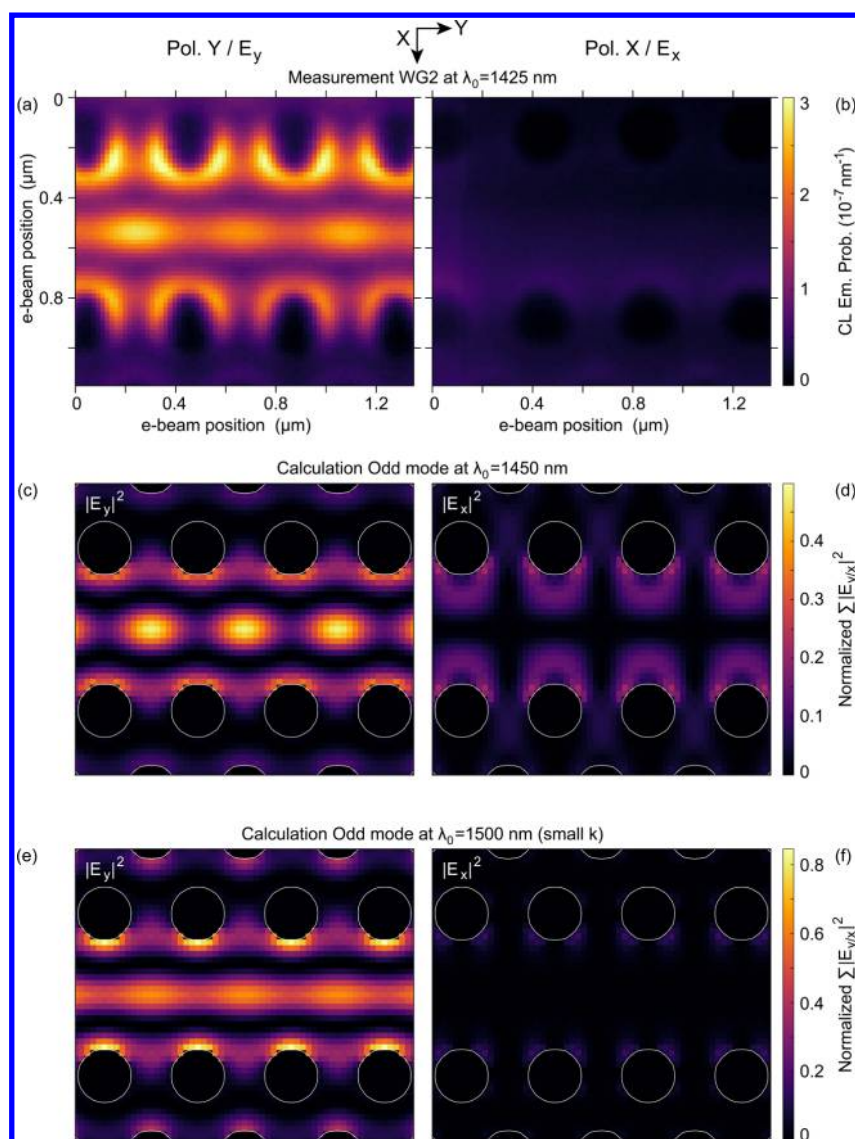
Figure 4. Polarization-filtered 2D excitation maps of WG2, showing the CL emission probability as a function of the electron beam position for a center wavelength of $\lambda_0 = 1425$ nm, averaged over a 20 nm bandwidth. Only a linear polarizer was used here. The polarization is horizontal along the waveguide (along y) for (a) and vertical (along x) for (b), and the two are shown on the same intensity scale. (c) Calculation of the field intensity $|E_y|^2$ for the odd waveguide mode at $\lambda_0 = 1450$ nm and the corresponding calculation for $|E_x|^2$ (d), integrated over k within the frequency range, both shown on the same scale normalized to the overall total maximum intensity for all the calculations. We show $|E_y|^2$ (e) and $|E_x|^2$ (f) on the same scale for the odd mode calculated at $\lambda_0 = 1500$ nm, integrated (within the frequency range) over a range of k close to 0, above the light line. The distributions for k below the light line can be seen in Figure S7 of the Supporting Information.

on the implementation can be found in the Methods section and the Supporting Information.

We display the Stokes parameters for excitation position A on WG2 oriented along the y-axis in Figure 3c. S0 corresponds to the total intensity, where we have not corrected for the emission from the substrate. S3 determines the ellipticity and handedness of the polarization. We do not expect circularly polarized emission from the structure, but for linearly polarized emission the measured reflection off of the curved surface of the mirror can lead to a circular component. This is negligible only if the slit that spatially filters the emission is positioned at the center of the parabolic mirror, where the emitted and reflected rays lie in the same plane as the surface normal of the mirror. In that case the problem reduces to classical Fresnel reflection where the s- and p-polarizations (horizontal and vertical) are conserved. We find that S3 ≈ 0 for all wavelengths,

demonstrating that the slit is well aligned. S2, which indicates the orientation of the principal axes of linearly polarized light, is also close to zero over all wavelengths. All of the polarized contribution is contained in S1, meaning that the polarization is fully linear and either horizontal (S1 > 0) or vertical (S1 < 0). Horizontal polarization corresponds to emission polarized along the y-axis, and vertical polarization corresponds to emission polarized along either the z-axis or the x-axis of the coordinate system (see Figure 1). We find that the dominant peak at $\lambda_0 = 1425$ nm is polarized along the waveguide axis (y-axis for data shown here). A TM mode predominantly has an out-of-plane electric field, i.e., along the z-axis, and would therefore be measured as a vertical polarization for any orientation of the waveguide. In-plane TE modes, with electric field components typically along the waveguide axis or orthogonal to it, will be along either the x- or y-axes for

carefully aligned orthogonal orientations of the waveguide. Their emission will be measured up as a horizontal polarization for one orientation and vertical for the other orthogonal orientation. Experiments using such orthogonal orientations of the waveguide (see Figure S6 of the Supporting Information) result in orthogonal horizontal/vertical polarizations for all of the measured peaks. This demonstrates that all of the features are related to TE and not to TM modes, confirming once again that the electron beam can couple to in-plane excitations.

Using polarimetry allows us to separate the polarized (in red) and unpolarized (in gray) contributions to the spectra from Figure 3c. Compared to the measured total intensity S0 we can clearly see that most of the signal, including the small peak at $\lambda_0 \approx 1275$ nm, is unpolarized. We ascribe this unpolarized emission to the luminescence from the substrate. The peaks in the polarized contribution all correspond to modal features in Figure 2 (for both excitation positions A and B) and demonstrates the power of polarimetry to filter out these unpolarized contributions to obtain clear resonances with a high contrast.

Figure 4a,b show measurements of the polarization-filtered CL emission intensity distributions from WG2, at $\lambda_0 = 1425$ nm, for x and y polarization. Clearly, the emission is polarized along the waveguide axis y. Figure 4c,d show the calculated modal field intensity distributions (summed over k) at $\lambda_0 = 1450$ nm for the E_y (c) and E_x (d) components. We observe good qualitative agreement between the calculations and the measurements, especially for the E_y component, while the calculated E_x intensity is more intense than the x-polarized data. At this wavelength the mode is guided, but it is close to the light line. The emission can still escape, due to scattering from roughness and imperfections for instance. The emission directionality toward the surface normal ($k \approx 0$) suggests, however, that the mode can radiate out directly, indicating that the leaky part of the odd mode contributes to the measured emission.

For this reason we also calculate the field profiles at $\lambda_0 = 1500$ nm, where the dispersion relation of the odd mode intersects the frequency window of the calculation for regions of k both above the light line (close to $k = 0$) and below the light line. The modal intensity distributions for k above the light line show very good agreement with the data, as we can observe in Figure 4e for the E_y intensity and in Figure 4f for the E_x intensity. The intensity profiles for k below the light line differ more from the measured emission profiles (see Figure S7 of the Supporting Information). Comparing the measurements to the calculations, we find that the intensity distributions and relative intensities (for both polarizations) show agreement for both calculations, but there is clearly a better match with the leaky distributions at $\lambda_0 = 1500$ nm. The discrepancy in wavelength between measurement and calculation can be attributed to variations between the measured and calculated geometrical parameters, which we have shown to strongly impact the positions of all resonances in the spectra. We note that the calculations are not designed to determine field profiles in the leaky region above the light line, since they do not take into account nonzero values of k_z, which necessarily exist for leaky modes that radiate out of the waveguide to free space. Calculations in other systems, however, that do fully take leaky contributions into account, have shown that the mode can retain its overall field profile, even if it does become more lossy.[59,60] In our case this is advantageous, as the mode is radiating out of the structure more freely, allowing us to measure it directly.

CL spectroscopy proves to be a useful technique to measure modes in nanophotonic structures, comparable to NSOM for example. In the case of NSOM, the near field is mapped with a nanoprobe that is brought into the evanescent field of the light in the nanostructure. As a result, different field components of both the electric and magnetic fields can be distinguished,[31,32] allowing in-depth studies of confined modes at the nanoscale, including their dispersion. However, the image formation is complex and the interpretation of the experimental results is nontrivial. The nanoprobes used to perform NSOM measurements can, in certain cases, perturb the system, so care must be taken in the processing and interpretation of the data. Another way to image confined modes is grating-assisted Fourier space imaging, in which light from below the light line is scattered to the far field by a secondary grating and collected by a Fourier lens.[61,62] This approach permits one to determine the dispersion relation, symmetry, and interaction of confined modes, but the secondary grating can also perturb the system similarly to the NSOM nanoprobes and adds additional complexity to the fabrication. CL on the other hand is a noninvasive far-field technique (the electrons excite, but do not perturb, the electromagnetic modes), measuring light both from leaky modes above the light line and from confined modes that scatter out due to defects. Unlike NSOM, CL also probes the fields inside a structure as the electrons travel through it. Additionally, the emission can be related to the radiative LDOS[36] and the excitation resolution is truly nanoscale (~10 nm).

CONCLUSIONS

In conclusion, we have demonstrated that an electron beam can be used to excite the propagating TE modes of a Si photonic crystal waveguide, despite them being dominated by in-plane field components. We applied, for the first time, spectroscopic cathodoluminescence imaging polarimetry in the near-infrared spectral range, to directly image the modal field distribution and image the emission and polarization with nanoscale resolution. Accordingly, the most striking feature that we observe is the odd TE waveguide mode of the structure, which exhibits a highly localized emission intensity distribution. Using spectroscopic polarimetry we demonstrate that the emission of this mode is fully linearly polarized along the direction of the waveguide. This is supported by calculations of the electric field intensities, which show good qualitative agreement with both the measured intensity distributions and polarization. Surprisingly, the vertically oriented electron beam can couple to this in-plane mode, as a result of nonzero contributions from the out-of-plane field component at different heights within the waveguide. A redistribution of the electron trajectories due to scattering also plays a role. The emission peak corresponding to the odd waveguide mode is directional toward the surface normal, indicating that we sample a leaky part of the waveguide mode that radiates out of the structure. Spectroscopic cathodoluminescence imaging polarimetry is a powerful, noninvasive tool to measure light confinement, polarization, and propagation at the nanoscale in photonic crystal waveguides and other complex nanophotonic structures.

■ METHODS

Cathodoluminescence Measurements. The measurements were performed in a FEI XL-30 SFEG (10–30 keV electron beam, ~30–46 nA current) equipped with a home-built CL system.[34,37,54] An aluminum parabolic mirror collects the emitted light and directs it outside of the microscope to an optical setup. We can measure the spectrum in the $\lambda_0 = 350$–1000 nm spectral range with a liquid-nitrogen-cooled back-illuminated silicon CCD array (Princeton Instruments Spec-10 100B) and in the $\lambda_0 = 900$–1600 nm spectral range with a liquid-nitrogen-cooled InGaAs photodiode array (Princeton Instruments OMA V). Due to the readout noise of the individual pixels, we smooth the spectra with a moving filter over a 2 nm bandwidth. We correct for the system response of the setup by using transition radiation from single-crystal aluminum as a reference.[58] A Faraday cup integrated in the sample holder measures the current of the electron beam, which in combination with the system response allows us to determine the CL emission probability. A quarter-wave plate (Thorlabs AQWP10M-1600) and linear polarizer (Moxtek PUBB01A50M) are used together to measure the full polarization state of the emitted radiation.[37] To measure the polarization, we place a 3 mm wide slit in the beam path followed by the QWP and Pol., which offers a good balance between signal intensity and polarization contrast.[55,56] Because we focus all of the light passing through the slit onto the spectrometer, the measured polarization is averaged over the zenithal angles that are collected. A series of six measurements for different combinations of the QWP and Pol. (horizontal/90°, vertical/0°, 45°, 135°, right- and left-handed circular) determine the Stokes parameters, which fully describe the polarization state of the light. Measurement errors can occur due to drift of the electron beam across the sample, bleaching, or contamination, leading to a reduction in the measured intensity, as well as fluctuations in the current and optical alignment of the mirror. For all spectral measurements we collect a dark reference spectrum where we blank the electron beam, subtracting this from the data in the postprocessing stage.

Calculations. To calculate the modal fields of the photonic crystal waveguide, we calculated the eigenfrequencies and complex field amplitudes $E(r)$ using the MIT Photonics Band code,[51] which is a plane-wave method that uses periodic boundary conditions to calculate the eigenfrequencies and eigenmodes of our PCWGs. The band structure diagrams were calculated with the full 3D version. In order to conserve computational resources, we implemented a 2D version of the calculation using an effective index approximation to determine the field profiles. The effective index of the slab was chosen to be that of a 220 nm thick slab of silicon with the refractive index appropriate for each frequency range considered (for example for wavelengths around $\lambda_0 = 1450$ nm, we used 3.484). This procedure yields an effective index of 2.873 for TE modes and 1.831 for TM modes at $\lambda_0 = 1450$ nm. We determine the eigenvalues between 99% and 101% of the desired frequency. The E_x, E_y, and E_z field profiles (or eigenmodes) are calculated on a rectangular grid of points separated by $a/16$, ensuring that the eigenfrequencies are converged to better than 0.1%. The modes are normalized such that $\int_{\text{unit cell}} \epsilon(r) |E(r)|^2 \, dr = 1$. The calculations are performed for wavevectors in the first irreducible Brillouin zone, after which we use symmetry arguments to add the fields for different wavevectors with the

correct weighting factor, over the full first Brillouin zone. Essentially, we sum the field intensities over all wavevectors $\mathbf{k}$ of the modes that occur within the frequency range of the calculation, at each position $\mathbf{r}$:

$$\frac{1}{(2\pi)^3} \sum_{n=1}^{N} \int_k |E_{n\mathbf{k}}^{(i)}(\mathbf{r})|^2 \delta(\omega - \omega_{n\mathbf{k})} \, d\mathbf{k}, \quad i = x, y, z \tag{1}$$

For the leaky/guided mode results we only sum over the wavevectors above/below the light line. The total field intensity is then determined by summing over all three field components. All of the resulting field intensity distributions are normalized to the maximum total intensity value for all wavelengths and polarizations (TE at $\lambda_0 = 1500$ nm). The intensity inside the holes is set to zero to better compare the results to the measurements, since there is no polarizable material in the empty holes and the electron beam does not produce radiation even if there can be a high field intensity and/or LDOS in the holes.

■ ASSOCIATED CONTENT

ⓢ Supporting Information

The Supporting Information is available free of charge on the ACS Publications website at DOI: 10.1021/acsphotonics.6b00557.

> Measured data from an additional sample, an input section of the waveguide studied here and for shorter wavelengths; 2D calculations for TM polarization, 3D calculations for TE polarization, and a comparison of the calculated field components of the even and odd waveguide modes; an explanation of the spectroscopic polarimetry method (PDF)

■ AUTHOR INFORMATION

Corresponding Author

*E-mail (A. Polman): polman@amolf.nl.

Notes

The authors declare the following competing financial interest(s): A.P. is co-founder and co-owner of Delmic BV, a startup company developing a commercial product based on the cathodoluminescence system that was used in this work.

■ ACKNOWLEDGMENTS

■ REFERENCES

(1) Yablonovitch, E. Inhibited spontaneous emission in solid-state physics and electronics. *Phys. Rev. Lett.* **1987**, *58*, 2059.

(2) Yablonovitch, E. Photonic band-gap structures. *J. Opt. Soc. Am. B* **1993**, *10*, 283–295.

(3) Blanco, A.; Chomski, E.; Grabtchak, S.; Ibisate, M.; John, S.; Leonard, S. W.; Lopez, C.; Meseguer, F.; Miguez, H.; Mondia, J. P.; Ozin, G. A.; Toader, O.; van Driel, H. M. Large-scale synthesis of a

silicon photonic crystal with a complete three-dimensional bandgap near 1.5 micrometres. *Nature* **2000**, *405*, 437−440.

(4) Fujita, M.; Takahashi, S.; Tanaka, Y.; Asano, T.; Noda, S. Simultaneous inhibition and redistribution of spontaneous light emission in photonic crystals. *Science* **2005**, *308*, 1296−1298.

(5) Joannopoulos, J. D.; Johnson, S. G.; Winn, J. N.; Meade, R. D. *Photonic Crystals: Molding the Flow of Light*; Princeton University Press, 2011.

(6) Yoshie, T.; Scherer, A.; Hendrickson, J.; Khitrova, G.; Gibbs, H. M.; Rupper, G.; Ell, C.; Shchekin, O. B.; Deppe, D. G. Vacuum Rabi splitting with a single quantum dot in a photonic crystal nanocavity. *Nature* **2004**, *432*, 200−203.

(7) Akahane, Y.; Asano, T.; Song, B.-S.; Noda, S. High-Q photonic nanocavity in a two-dimensional photonic crystal. *Nature* **2003**, *425*, 944−947.

(8) Hughes, S. Enhanced single-photon emission from quantum dots in photonic crystal waveguides and nanocavities. *Opt. Lett.* **2004**, *29*, 2659−2661.

(9) Noda, S.; Yokoyama, M.; Imada, M.; Chutinan, A.; Mochizuki, M. Polarization mode control of two-dimensional photonic crystal laser by unit cell structure design. *Science* **2001**, *293*, 1123−1125.

(10) Park, H.-G.; Kim, S.-H.; Kwon, S.-H.; Ju, Y.-G.; Yang, J.-K.; Baek, J.-H.; Kim, S.-B.; Lee, Y.-H. Electrically driven single-cell photonic crystal laser. *Science* **2004**, *305*, 1444−1447.

(11) Hirose, K.; Liang, Y.; Kurosaka, Y.; Watanabe, A.; Sugiyama, T.; Noda, S. Watt-class high-power, high-beam-quality photonic-crystal lasers. *Nat. Photonics* **2014**, *8*, 406−411.

(12) Liles, A. A.; Debnath, K.; O'Faolain, L. Lithographic wavelength control of an external cavity laser with a silicon photonic crystal cavity-based resonant reflector. *Opt. Lett.* **2016**, *41*, 894−897.

(13) Krauss, T. F. Slow light in photonic crystal waveguides. *J. Phys. D: Appl. Phys.* **2007**, *40*, 2666.

(14) Krauss, T. F.; Richard, M.; Brand, S. Two-dimensional photonic-bandgap structures operating at near-infrared wavelengths. *Nature* **1996**, *383*, 699−702.

(15) Notomi, M.; Yamada, K.; Shinya, A.; Takahashi, J.; Takahashi, C.; Yokohama, I. Extremely large group-velocity dispersion of line-defect waveguides in photonic crystal slabs. *Phys. Rev. Lett.* **2001**, *87*, 253902.

(16) Vlasov, Y. A.; O'Boyle, M.; Hamann, H. F.; McNab, S. J. Active control of slow light on a chip with photonic crystal waveguides. *Nature* **2005**, *438*, 65−69.

(17) Mazoyer, S.; Baron, A.; Hugonin, J.-P.; Lalanne, P.; Melloni, A. Slow pulses in disordered photonic-crystal waveguides. *Appl. Opt.* **2011**, *50*, G113−G117.

(18) Beggs, D. M.; Rey, I. H.; Kampfrath, T.; Rotenberg, N.; Kuipers, L.; Krauss, T. F. Ultrafast tunable optical delay line based on indirect photonic transitions. *Phys. Rev. Lett.* **2012**, *108*, 213901.

(19) Gersen, H.; Karle, T.; Engelen, R.; Bogaerts, W.; Korterik, J.; Van Hulst, N.; Krauss, T.; Kuipers, L. Real-space observation of ultraslow light in photonic crystal waveguides. *Phys. Rev. Lett.* **2005**, *94*, 073903.

(20) Baba, T. Slow light in photonic crystals. *Nat. Photonics* **2008**, *2*, 465−473.

(21) Morichetti, F.; Ferrari, C.; Canciamilla, A.; Melloni, A. The first decade of coupled resonator optical waveguides: bringing slow light to applications. *Laser Photonics Rev.* **2012**, *6*, 74−96.

(22) Melloni, A.; Canciamilla, A.; Ferrari, C.; Morichetti, F.; O'Faolain, L.; Krauss, T.; De La Rue, R.; Samarelli, A.; Sorel, M. Tunable delay lines in silicon photonics: coupled resonators and photonic crystals, a comparison. *IEEE Photonics J.* **2010**, *2*, 181−194.

(23) Zabelin, V.; Dunbar, L. A.; Le Thomas, N.; Houdré, R.; Kotlyar, M. V.; O'Faolain, L.; Krauss, T. F. Self-collimating photonic crystal polarization beam splitter. *Opt. Lett.* **2007**, *32*, 530−532.

(24) Beggs, D. M.; White, T. P.; O'Faolain, L.; Krauss, T. F. Ultracompact and low-power optical switch based on silicon photonic crystals. *Opt. Lett.* **2008**, *33*, 147−149.

(25) Corcoran, B.; Monat, C.; Grillet, C.; Moss, D. J.; Eggleton, B. J.; White, T.; O'Faolain, L.; Krauss, T. F. Green light emission in silicon through slow-light enhanced third-harmonic generation in photonic-crystal waveguides. *Nat. Photonics* **2009**, *3*, 206−210.

(26) Pohl, D. W.; Denk, W.; Lanz, M. Optical stethoscopy: Image recording with resolution λ/20. *Appl. Phys. Lett.* **1984**, *44*, 651−653.

(27) Betzig, E.; Trautman, J. K.; Harris, T. D.; Weiner, J. S.; Kostelak, R. L. Breaking the diffraction barrier: optical microscopy on a nanometric scale. *Science* **1991**, *251*, 1468−1470.

(28) Reddick, R. C.; Warmack, R. J.; Ferrell, T. L. New form of scanning optical microscopy. *Phys. Rev. B: Condens. Matter Mater. Phys.* **1989**, *39*, 767.

(29) Chicanne, C.; David, T.; Quidant, R.; Weeber, J.-C.; Lacroute, Y.; Bourillot, E.; Dereux, A.; Colas des Francs, G.; Girard, C. Imaging the local density of states of optical corrals. *Phys. Rev. Lett.* **2002**, *88*, 097402.

(30) Colas des Francs, G.; Girard, C.; Weeber, J.-C.; Dereux, A. Relationship between scanning near-field optical images and local density of photonic states. *Chem. Phys. Lett.* **2001**, *345*, 512−516.

(31) Novotny, L. The history of near-field optics. *Prog. Opt.* **2007**, *50*, 137.

(32) Le Feber, B.; Rotenberg, N.; Beggs, D. M.; Kuipers, L. Simultaneous measurement of nanoscale electric and magnetic optical fields. *Nat. Photonics* **2014**, *8*, 43−46.

(33) García de Abajo, F. J. Optical excitations in electron microscopy. *Rev. Mod. Phys.* **2010**, *82*, 209−275.

(34) Sapienza, R.; Coenen, T.; Renger, J.; Kuttge, M.; van Hulst, N. F.; Polman, A. Deep-subwavelength imaging of the modal dispersion of light. *Nat. Mater.* **2012**, *11*, 781−787.

(35) Brenny, B. J. M.; Polman, A.; García de Abajo, F. J. Femtosecond plasmon and photon wave packets excited by a high-energy electron on a metal or dielectric surface. *Phys. Rev. B: Condens. Matter Mater. Phys.* **2016**, *94*, 155412.

(36) Losquin, A.; Kociak, M. Link between cathodoluminescence and electron energy loss spectroscopy and the radiative and full electromagnetic local density of states. *ACS Photonics* **2015**, *2*, 1619−1627.

(37) Osorio, C. I.; Coenen, T.; Brenny, B. J. M.; Polman, A.; Koenderink, A. F. Angle-resolved cathodoluminescence imaging polarimetry. *ACS Photonics* **2016**, *3*, 147−154.

(38) Spirkoska, D.; et al. Structural and optical properties of high quality zinc-blende/wurtzite GaAs nanowire heterostructures. *Phys. Rev. B: Condens. Matter Mater. Phys.* **2009**, *80*, 245325.

(39) Zhu, X. L.; Ma, J. S.; Zhang, Y.; Xu, X. F.; Wu, J.; Zhang, Y.; Han, X. B.; Fu, Q.; Liao, Z. M.; Chen, L.; Yu, D. P. Confined three-dimensional plasmon modes inside a ring-shaped nanocavity on a silver film imaged by cathodoluminescence microscopy. *Phys. Rev. Lett.* **2010**, *105*, 127402.

(40) Bashevoy, M. V.; Jonsson, F.; MacDonald, K. F.; Chen, Y.; Zheludev, N. I. Hyperspectral imaging of plasmonic nanostructures with nanoscale resolution. *Opt. Express* **2007**, *15*, 11313−11320.

(41) Adamo, G.; Ou, J. Y.; So, J. S.; Jenkins, S. D.; De Angelis, F.; MacDonald, K. F.; Di Fabrizio, E.; Ruostekoski, J.; Zheludev, N. I. Electron-beam-driven collective-mode metamaterial light source. *Phys. Rev. Lett.* **2012**, *109*, 217401.

(42) Yamamoto, N.; Ohtani, S.; García de Abajo, F. J. Gap and Mie plasmons in individual silver nanospheres near a silver surface. *Nano Lett.* **2011**, *11*, 91−95.

(43) Myroshnychenko, V.; Nelayah, J.; Adamo, G.; Geuquet, N.; Rodríguez-Fernández, J.; Pastoriza-Santos, I.; MacDonald, K. F.; Henrard, L.; Liz-Marzán, L. M.; Zheludev, N. I.; Kociak, M.; García de Abajo, F. J. Plasmon spectroscopy and imaging of individual gold nanodecahedra: a combined optical microscopy, cathodoluminescence, and electron energy-loss spectroscopy study. *Nano Lett.* **2012**, *12*, 4172−4180.

(44) Knight, M. W.; Liu, L.; Wang, Y.; Brown, L.; Mukherjee, S.; King, N. S.; Everitt, H. O.; Nordlander, P.; Halas, N. J. Aluminum plasmonic nanoantennas. *Nano Lett.* **2012**, *12*, 6000−6004.

(45) Takeuchi, K.; Yamamoto, N. Visualization of surface plasmon polariton waves in two-dimensional plasmonic crystal by cathodoluminescence. *Opt. Express* **2011**, *19*, 12365−12374.

(46) Honda, M.; Yamamoto, N. Size dependence of surface plasmon modes in one-dimensional plasmonic crystal cavities. *Opt. Express* **2013**, *21*, 11973−11983.

(47) Ma, X.; Grüßer, M.; Schuster, R. Angular Dependence of Cathodoluminescence of Linear and Circular Au Gratings: Imaging the Coupling Angles between Surface Plasmon Polaritons and Light. *J. Phys. Chem. C* **2014**, *118*, 23247−23255.

(48) Benisty, H. Modal analysis of optical guides with two-dimensional photonic band-gap boundaries. *J. Appl. Phys.* **1996**, *79*, 7483−7492.

(49) Johnson, S. G.; Villeneuve, P. R.; Fan, S.; Joannopoulos, J. D. Linear waveguides in photonic-crystal slabs. *Phys. Rev. B: Condens. Matter Mater. Phys.* **2000**, *62*, 8212.

(50) Lecamp, G.; Hugonin, J.-P.; Lalanne, P. Theoretical and computational concepts for periodic optical waveguides. *Opt. Express* **2007**, *15*, 11042−11060.

(51) Johnson, S. G.; Joannopoulos, J. D. Block-iterative frequency-domain methods for Maxwell's equations in a planewave basis. *Opt. Express* **2001**, *8*, 173−190.

(52) Beggs, D. M.; O'Faolain, L.; Krauss, T. F. Accurate determination of the functional hole size in photonic crystal slabs using optical methods. *Phot. Nano. Fundam. Appl.* **2008**, *6*, 213−218.

(53) Lončar, M.; Nedeljković, D.; Pearsall, T. P.; Vučković, J.; Scherer, A.; Kuchinsky, S.; Allan, D. C. Experimental and theoretical confirmation of Bloch-mode light propagation in planar photonic crystal waveguides. *Appl. Phys. Lett.* **2002**, *80*, 1689−1691.

(54) Coenen, T.; Vesseur, E. J. R.; Polman, A. Angle-resolved cathodoluminescence spectroscopy. *Appl. Phys. Lett.* **2011**, *99*, 143103.

(55) Vesseur, E. J. R.; Polman, A. Plasmonic whispering gallery cavities as optical antennas. *Nano Lett.* **2011**, *11*, 5524−5530.

(56) Coenen, T.; Polman, A. Polarization-sensitive cathodoluminescence Fourier microscopy. *Opt. Express* **2012**, *20*, 18679−19691.

(57) Born, M.; Wolf, E. *Principles of Optics: Electromagnetic Theory of Propagation, Interference and Diffraction of Light*, 7th ed.; Cambridge University Press, 1997.

(58) Brenny, B. J. M.; Coenen, T.; Polman, A. Quantifying coherent and incoherent cathodoluminescence in semiconductors and metals. *J. Appl. Phys.* **2014**, *115*, 244307.

(59) Paniagua-Domínguez, R.; Grzela, G.; Gómez Rivas, J.; Sánchez-Gil, J. Enhanced and directional emission of semiconductor nanowires tailored through leaky/guided modes. *Nanoscale* **2013**, *5*, 10582−10590.

(60) Abujetas, D. R.; Paniagua-Domínguez, R.; Sánchez-Gil, J. A. Unraveling the janus role of Mie resonances and leaky/guided modes in semiconductor nanowire absorption for enhanced light harvesting. *ACS Photonics* **2015**, *2*, 921−929.

(61) Le Thomas, N.; Houdré, R.; Frandsen, L. H.; Fage-Pedersen, J.; Lavrinenko, A. V.; Borel, P. I. Grating-assisted superresolution of slow waves in Fourier space. *Phys. Rev. B: Condens. Matter Mater. Phys.* **2007**, *76*, 035103.

(62) Jágerská, J.; Le Thomas, N.; Houdré, R.; Beggs, D. M.; O'Brien, D.; Krauss, T. F. Coupling length of silicon-on-insulator directional couplers probed by Fourier-space imaging. *Appl. Phys. Lett.* **2008**, *92*, 151106.